







RESEARCH ARTICLE | JUNE 03 2022

## Simplified CVD route to near-zero thickness silicon nitride films

Barry Arkles  ; Chad Brick  ; Jonathan Goff  ; Alain E. Kaloyeros 



*J. Vac. Sci. Technol. B* 40, 040601 (2022)

<https://doi.org/10.1116/6.0001820>



# Simplified CVD route to near-zero thickness silicon nitride films

Cite as: J. Vac. Sci. Technol. B 40, 040601 (2022); doi: 10.1116/6.0001820

Submitted: 23 February 2022 · Accepted: 10 May 2022 ·

Published Online: 3 June 2022



Barry Arkles,<sup>1,a)</sup> Chad Brick,<sup>2</sup> Jonathan Goff,<sup>2</sup> and Alain E. Kaloyeros<sup>3</sup>

## AFFILIATIONS

<sup>1</sup>Department of Chemistry, Temple University, Philadelphia, Pennsylvania 19122

<sup>2</sup>Gelast Inc., 11 Steel Road East, Morrisville, Pennsylvania 19067

<sup>3</sup>BFD Innovation, Slingerlands, New York 12159

<sup>a)</sup>Electronic mail: [barry.arkles@temple.edu](mailto:barry.arkles@temple.edu)

## ABSTRACT

Silicon nitride ( $\text{SiN}_x$ ,  $x \sim 1$ ) thin films were deposited by chemical vapor deposition on silicon oxide ( $\text{SiO}_2$ ) substrates by combining controlled pulses of the precursor 1,3,5-tri(isopropyl)cyclotrisilazane (TICZ,  $\text{C}_9\text{H}_{27}\text{N}_3\text{Si}_3$ ) with a continuous ammonia ( $\text{NH}_3$ ) plasma. This plasma-assisted pulsed CVD (PPCVD) process enables the integration of the nanoscale thickness and uniformity control achieved in atomic layer deposition with the efficiency of plasma-enhanced CVD (PE-CVD). TICZ was selected because it is a nonpyrophoric stable liquid with a high vapor pressure ( $\sim 133$  Pa at  $70^\circ\text{C}$ ) and could act as a single source for  $\text{SiN}_x$  with both high Si and N contents. An optimized PPCVD process window was identified consisting of a substrate temperature of  $350^\circ\text{C}$ , a TICZ pulse of  $\leq 0.2$  s, and a TICZ purge pulse  $\geq 10$  s in a continuous direct  $\text{NH}_3$  plasma at a  $\text{NH}_3$  flow rate and a power of 40 SCCM and 3000 W, respectively. The as-deposited films were analyzed by x-ray photoelectron spectroscopy (XPS) and spectroscopic ellipsometry. XPS analysis confirmed the absence of any C inclusion and demonstrated the existence of the 1:1 Si:N ratio. *In situ*, real-time ellipsometry measurements indicated that  $\text{SiN}_x$  growth occurred in a typical PE-CVD regime. They also yielded an as-grown  $\text{SiN}_x$  average refractive index of  $\sim 1.75$ .

© 2022 Author(s). All article content, except where otherwise noted, is licensed under a Creative Commons Attribution (CC BY) license (<http://creativecommons.org/licenses/by/4.0/>). <https://doi.org/10.1116/6.0001820>

## I. INTRODUCTION

The silicon nitride ( $\text{SiN}_x$ ,  $1 < x < 1.33$ ) material system continues to receive significant scientific and industrial attention due to its highly desirable physical, chemical, electrical, and biological properties.<sup>1–3</sup> These properties have led to a long-established history of inclusion of  $\text{SiN}_x$  thin films in a multitude of technical applications in the semiconductor, photovoltaic, and optical fields. While these traditional usages continue unabated, a plethora of new exciting applications are being actively explored. These applications include diffusion barriers, glue and passivation layers, and antireflection coatings in emerging nanoscale integrated circuitry and solar cell devices; base anchors for nanophotonic quantum dots and nanoscale crystals;<sup>4,5</sup> nonlinear waveguides for telecommunication optical sensors and devices;<sup>6</sup> tunable light-emitters for light emitting diodes;<sup>7</sup> passivation/encapsulation layers in compound semiconductor devices;<sup>8</sup> and host matrices for biological and biochemical materials for medical applications.<sup>9,10</sup>

All these applications, whether intended to extend the use of  $\text{SiN}_x$  in traditional technologies or incorporate it in novel and emerging usages, do share the common theme of consisting of heterodevice structures built on thermally sensitive and/or chemically delicate substrates.<sup>11–15</sup> The vapor phase deposition of  $\text{SiN}_x$  on these substrates requires a low thermal budget and chemically inert precursors to eliminate or minimize any resulting damage to the fragile nanoscale device assemblies. To achieve these goals, potential solutions have included the introduction of new chemical sources with lower decomposition temperatures<sup>16–18</sup> and the use of nonthermal energy sources such as direct and remote plasma,<sup>19</sup> tunable laser,<sup>20</sup> and unique chamber architectures.<sup>8,14,21</sup> The overarching strategy has been to achieve low-temperature growth of  $\text{SiN}_x$  thin films in processes that fall under the main categories of chemical vapor deposition (CVD) and atomic layer deposition (ALD).

Unfortunately, a number of issues still prevent the successful integration of  $\text{SiN}_x$  into fragile and sensitive heterodevice systems. In the case of thermal CVD, these challenges are primarily of

30 April 2024 19:39:08

chemical nature related to the pyrophoricity, high decomposition temperature, and the incorporation of carbon (C) and hydrogen (H) contaminants in the resulting films.<sup>8,20–23</sup> In the case of plasma processes such as plasma-enhanced CVD (PE-CVD) and plasma-enhanced ALD (PE-ALD), the SiN<sub>x</sub> films tend to be nonstoichiometric and consist of either a Si- or N-rich phase and/or display poor homogeneity, in the sense that they exhibit a varying Si/N ratio throughout the film from the interface with the substrate to the film surface. The films were also reported to display a porous structure and include high concentrations of C, H, and O.<sup>7,24</sup> Practically, these challenges demonstrate that predictable and consistent film quality and performance are difficult since even if reproducibility is achieved within a specific heterodevice architecture, the results cannot be extrapolated to dissimilar designs.

To address these issues, the current investigators have been studying Si source precursors of the type *N*-alkyl substituted perhydridocyclotrisilazanes, which are designed with alkyl groups that could be eliminated using a low energy source.<sup>25,26</sup> In this context, this short communication is part of a series of studies by the present authors that aim to combine various low-energy sources with customized vapor phase deposition processes to enable high-quality SiN<sub>x</sub> growth from perhydridocyclotrisilazane precursor 1,3,5-tri(isopropyl)cyclotrisilazane (TICZ, C<sub>9</sub>H<sub>27</sub>N<sub>3</sub>Si<sub>3</sub>) at substrate temperatures below 400 °C.

Our prior reports have focused on the development of remote-plasma-activated pulsed CVD that incorporates thermal TICZ adsorption pulses and remote NH<sub>3</sub> plasma reaction pulses. The intent was to blend the advantages of precursor thermal adsorption, which promotes substrate-surface enabled conformal coating in nanoscale device topographies with the benefits of remote NH<sub>3</sub> plasma that activates both the precursor reaction and the substrate surface with radical species generated from ammonia, leading to the low temperature formation of SiN<sub>x</sub> thin films.<sup>27,28</sup>

In this short communication, we extend our work to the design of a plasma-assisted pulsed CVD (PPCVD) process that integrates controlled pulses of the TICZ precursor with a continuous ammonia (NH<sub>3</sub>) plasma. This PPCVD approach combines the nanoscale thickness and uniformity control achieved in ALD with the efficiency of a constant NH<sub>3</sub> plasma supply, including requiring only half the number of pulses per cycle required in conventional ALD. This simplified process enables the low-temperature formation of near-zero-thickness SiN<sub>x</sub> in a manufacturing-worthy throughput mode that is more conducive to inclusion in prevailing industrial protocols. To this end, concise results are presented from the development and optimization of a SiN<sub>x</sub> PPCVD process window. The as-deposited films were analyzed by x-ray photoelectron spectroscopy (XPS) and spectroscopic ellipsometry. The findings are summarized and discussed below.

## II. EXPERIMENT

### A. Materials

Tri(isopropyl)cyclotrisilazane precursor synthesis procedure and vapor pressure curve were previously reported elsewhere.<sup>27,28</sup> To summarize, it was determined that TICZ exhibited a highly adequate vapor pressure with a value of ~133 Pa at 70 °C, rising to over 500 Pa at 80 °C and reaching nearly 800 Pa at 90 °C. Nitrogen

with an initial purity estimated at 99.998% was purified during delivery using an activated nickel reduction process to levels of H<sub>2</sub>O, O<sub>2</sub>, CO, and CO<sub>2</sub> less than 100 pptV.

### B. PPCVD processing conditions

As with precursor synthesis, pertinent details pertaining to the PPCVD equipment were provided earlier and will only be summarized herein.<sup>27,28</sup>

All depositions were performed in a Picosun R-200 R&D tool consisting of a 200 mm-wafer reactor coupled with a load-lock system to ensure constant vacuum integrity and environmental isolation of the reaction chamber. Plasma power was generated by a remote inductively coupled plasma (ICP) power supply. Experiments were carried out on 1000 nm-thick silicon dioxide thermally deposited on n-doped Si wafers. The TICZ precursor bubbler was heated to 50 °C, while delivery lines were maintained at 90 °C. N<sub>2</sub> carrier gas was employed at 100 SCCM flow rate.

A demonstration of the feasibility study was initially carried out to establish specific cause and effect relationships between experimental conditions and resulting film properties. This study led to the identification of the most relevant deposition parameters with the ensuing information being applied to develop an optimum process window for the growth of the highest-quality SiN<sub>x</sub> thin films. The optimized deposition conditions are presented in Fig. 1 and summarized in Table I.

Under nonoptimized conditions, the films exhibit nonstoichiometric composition (typically Si-rich) and varying degrees of C contamination with C concentration being inversely proportional to substrate temperature (i.e., higher C inclusion with lower substrate temperature), which is expected due to the lack of the thermal energy required for complete precursor decomposition.

### C. Analytical techniques

The ellipsometer and XPS systems, as well as the *in situ* ellipsometry and *ex situ* XPS measurement techniques were described in detail in prior reports and are summarized here.<sup>27,28</sup> A Woollam iSE ellipsometer was employed for *in situ*, real-time, angle-resolved ellipsometry, in the wavelength range from 400 to 1000 nm. The angle utilized in the system is 60.8°. A CompleteEASE software package was applied for data analysis. Cauchy data modeling and analysis were performed with the substrate being treated as a ~1000 nm thick thermal SiO<sub>2</sub> film on Si with each individual SiO<sub>2</sub> layer thickness being evaluated *in situ* before every PPCVD experiment.

A PHI Quantum 2000 system was used for XPS studies. The resulting data were analyzed with a CASAXPS software package, with XPS plots production being performed with MultiPak software. Quantitative XPS elemental concentrations were calibrated by performing identical measurements simultaneously on a standard sputter-deposited silicon nitride sample of known composition.

## III. RESULTS AND DISCUSSION

### A. XPS analysis

Figure 2 presents a typical XPS depth profile for the Si, N, C, and O elemental concentrations versus penetration depth for

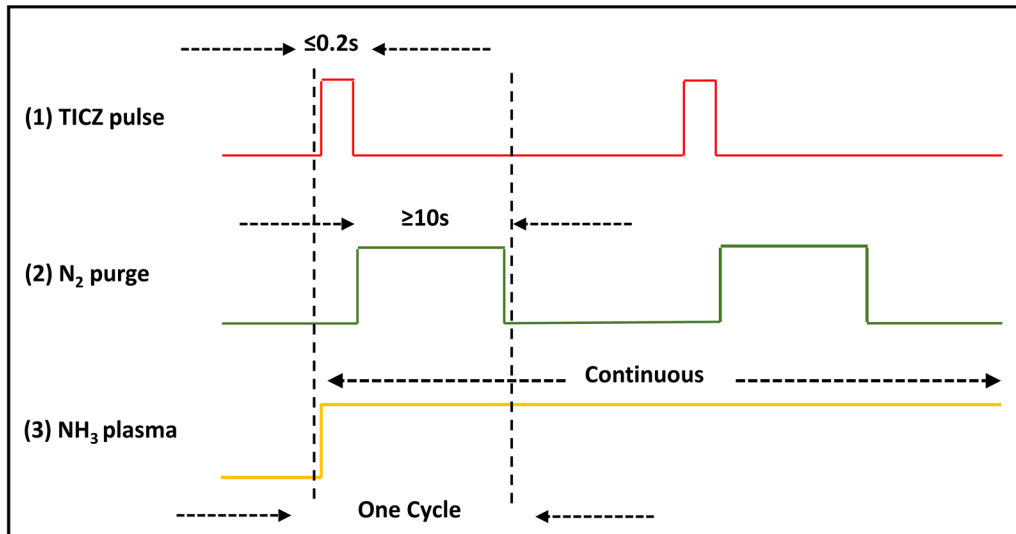


FIG. 1. Optimized PPCVD Si<sub>x</sub> process window.

as-deposited Si<sub>x</sub> films grown using the optimized processing window shown in Table I. XPS analyses indicate the complete absence of any C contamination in the PPCVD films, while O concentration was measured to be ~4–5 at.% after accounting for residual background O in the XPS system. The presence of oxygen could be ascribed to the well-documented plasma etching phenomenon of the Al<sub>2</sub>O<sub>3</sub> dielectric liners that are employed to confine the plasma in the ICP plasma source.<sup>29–31</sup> Furthermore, the XPS quantitative measurements yielded a 1:1 Si:N ratio in the as-deposited Si<sub>x</sub> films as observed in Fig. 2.

Also, Figs. 3(a)–3(d) exhibit the high-resolution XPS spectra for Si 2p, N 1s, C 1s, and O 1s binding energies, respectively, for Si<sub>x</sub> films deposited using the optimum process parameters listed in Table I. The location of the Si 2p and N 1s peaks at ~101.8 and ~398.1 eV, respectively, correspond to Si–N bonding configuration. The C 1s peak is at the background intensity level within the XPS detection limits, indicating the absence of C contaminants in the films. The small O 1s peak located at ~532.5 eV could be attributed to Si–O and/or N–O bonding arrangements.

TABLE I. Optimum PPCVD deposition parameters.

Parameter	Value
Substrate temperature	350 °C
TICZ pulse duration	≤0.2 s
TICZ purge pulse	≥10 s
Purge gas	N <sub>2</sub>
NH <sub>3</sub> plasma mode	Continuous
NH <sub>3</sub> flow rate	40 SCCM
NH <sub>3</sub> plasma power	3000 W

### B. Ellipsometry analysis

Film thicknesses versus deposition time are shown in Fig. 4 as compiled by *in situ*, real-time ellipsometry for Si<sub>x</sub> samples grown at varying precursor pulse and purge durations, while maintaining plasma power and a constant substrate temperature at 3000 W and 350 °C, respectively. Refractive index measurements were at 632.8 nm, as determined at the maximum thickness for the films using the Cauchy model.

As Fig. 4 demonstrates, film nucleation and growth begin immediately with the first precursor pulse, without the occurrence of the incubation period or delay that have typically plagued CVD and ALD SiN processes that employed non-*N*-alkyl substituted

30 April 2024 19:39:08

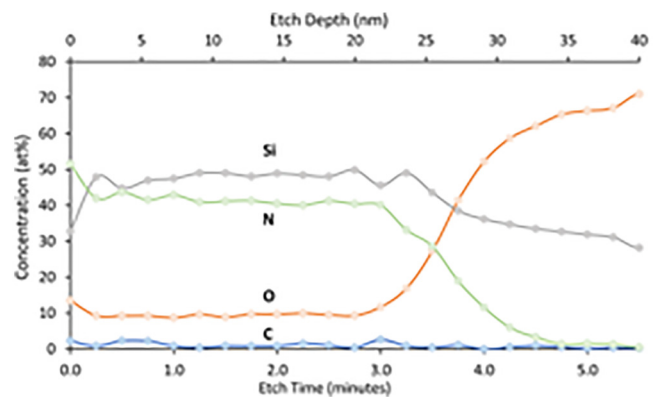


FIG. 2. XPS depth profile of Si, N, C, and O concentrations vs penetration depth in Si<sub>x</sub> for films deposited using the optimized PPCVD Si<sub>x</sub> process window.

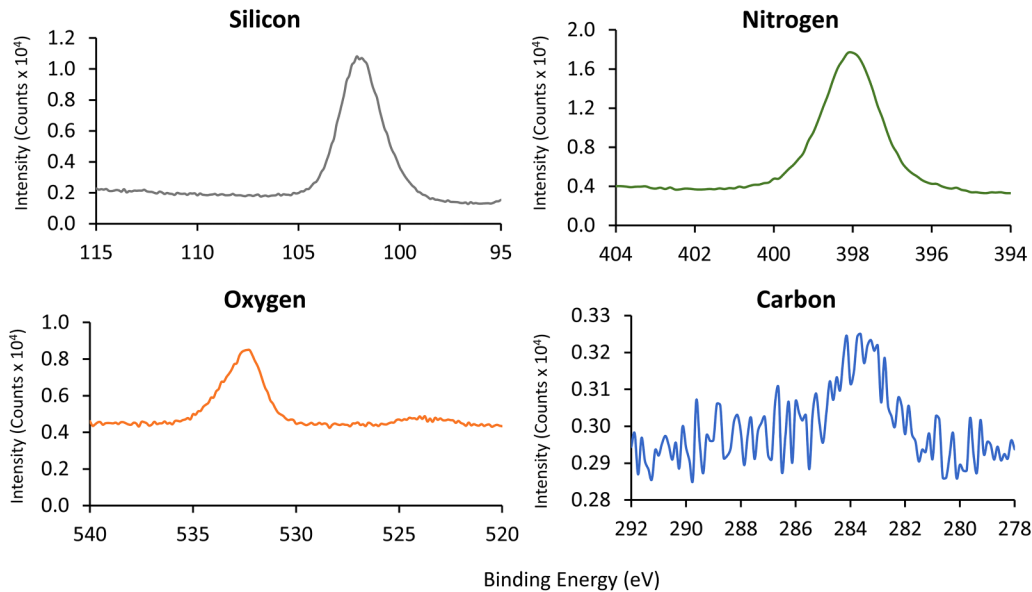


FIG. 3. Typical high-resolution XPS spectrum for (a) Si 2p; (b) N 1s; (c) C 1s; and (d) O 1s in SiN<sub>x</sub> films.

perhydridocyclotrisilazanes as Si source precursors.<sup>1,3</sup> Film thickness can be measured starting at the nonzero time coordinate, instead of the typically observed delay in film nucleation and growth due to the incubation period. This beneficial aspect of the PPCVD strategy is attributed to the efficiency of the TICZ precursor adsorption and decomposition pathways, as discussed in prior reports,<sup>25,26</sup> combined with the effective substrate surface pretreatment provided by the NH<sub>3</sub> plasma. The pretreatment has been shown to form a high density of highly reactive H and NH<sub>x</sub> (x = 1 or 2) species on the substrate surface, leading to increased reactivity with the Si source precursor.

Additionally, Table II lists representative growth rates per precursor pulse as a function of varying TICZ pulse duration and TICZ purge time. As can be seen in the table, the growth rate per precursor pulse is the highest for the lowest precursor

TABLE II. Representative growth rates as a function of processing parameters.

Substrate T (°C)	Parameter				Growth rate (per precursor pulse) (nm)
	NH <sub>3</sub> plasma power (W)	NH <sub>3</sub> flow rate (SCCM)	TICZ pulse duration (s)	TICZ purge duration (s)	
350	3000	40	0.2	10	~0.041
350	3000	40	0.2	20	~0.054
350	3000	40	0.1	10	~0.097

30 April 2024 19:39:08

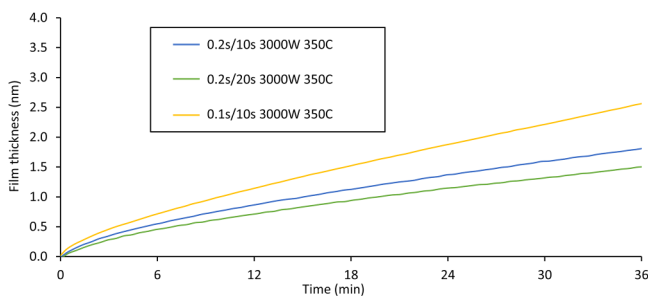


FIG. 4. *In situ*, real-time, ellipsometry measurements of film thickness vs deposition time as a function of varying TICZ pulse duration and TICZ purge time.

concentration (shortest residence time) in the reaction zone. This behavior seems to imply that substrate surface saturation is achieved at that value, thus resulting in the most efficient rate for precursor decomposition and film formation, with any excess precursor not contributing to the reaction. Also, the growth rate per precursor pulse does support the assertion that the PPCVD approach provides the atomic level thickness control needed for near-zero-thickness thin film applications. Ellipsometry also yielded an as-grown SiN<sub>x</sub> average refractive index of ~1.75 at 632.8 nm.

#### IV. CONCLUSIONS

This exploratory report presents critical results from the design and implementation of a simplified manufacturing process for ultrathin SiN<sub>x</sub> films that provides control similar to ALD but with less complexity (only half the number of pulses per cycle required in conventional ALD) and without incubation. The

plasma-assisted pulsed CVD (PPCVD) process that integrates controlled pulses of the TICZ precursor with continuous ammonia ( $\text{NH}_3$ ) plasma using the reaction of the source precursor 1,3,5-tri(isopropyl)cyclotrisilazane (TICZ,  $\text{C}_9\text{H}_{27}\text{N}_3\text{Si}_3$ ) with remote  $\text{NH}_3$  plasma. As such, the PPCVD process represents the second element in our strategy to develop and optimize high-quality  $\text{SiN}_x$  processes that integrate a low substrate thermal budget with chemically inert precursors for incorporation in the fragile nanoscale assemblies that form the basis for heterodevice structures. An optimized PPCVD process window is identified consisting of a substrate temperature of  $350^\circ\text{C}$ ; a TICZ pulse of  $\leq 0.2$  s; and a TICZ purge pulse  $\geq 10$  s in continuous direct  $\text{NH}_3$  plasma at a  $\text{NH}_3$  flow rate and a power of 40 SCCM and 3000 W, respectively. The resulting films are C-free and consist of the 1:1 Si:N ratio and are deposited at PPCVD growth rates per precursor pulse that support the assertion that the PPCVD approach provides the atomic level thickness control needed for near-zero-thickness thin film applications.

## AUTHOR DECLARATIONS

### Conflict of Interest

The authors have no conflicts to disclose.

## DATA AVAILABILITY

The data that support the findings of this study are available from the corresponding author upon reasonable request.

## REFERENCES

- <sup>1</sup>A. E. Kaloyeros, F. A. Jové, J. Goff, and B. Arkles, *ECS J. Solid State Sci. Technol.* **6**, P691 (2017).
- <sup>2</sup>N. Hegedüs, K. Balázs, and C. Balázs, *Materials* **14**, 5658 (2021).
- <sup>3</sup>A. E. Kaloyeros, J. D. Goff, Y. Pan, and B. Arkles, *ECS J. Solid State Sci. Technol.* **9**, 063006 (2020).
- <sup>4</sup>T. Torchynska, L. Khomenkova, and A. Slaoui, *J. Electron. Mater.* **47**, 3927 (2018).
- <sup>5</sup>S. Meziani, A. Moussi, L. Mahiou, F. Antoni, and R. Outemzabet, *Surf. Eng.* **36**, 456 (2020).
- <sup>6</sup>R. Kou *et al.*, *J. Appl. Phys.* **126**, 133101 (2019).
- <sup>7</sup>P. Zhang, L. Zhang, Y. Wu, S. Wang, and X. Ge, *Opt. Express* **26**, 31617 (2018).
- <sup>8</sup>Y. K. Ezhovskii and S. V. Mikhailovskii, *Russ. Microelectron.* **48**, 229 (2019).
- <sup>9</sup>T. Nagatsuka *et al.*, *Sens. Actuators B* **246**, 937 (2017).
- <sup>10</sup>B. Yin *et al.*, *ACS Omega* **2**, 7127 (2017).
- <sup>11</sup>A. E. Kaloyeros, J. D. Goff, and B. Arkles, *Electrochem. Soc. Interface* **27**, 59 (2018).
- <sup>12</sup>A. E. Kaloyeros, Y. Pan, J. Goff, and B. Arkles, *ECS J. Solid State Sci. Technol.* **8**, P119 (2019).
- <sup>13</sup>C. Brick, J. D. Goff, A. E. Kaloyeros, and B. Arkles, *ALD/ALE 2019*, Bellevue, WA, July 22–24, 2019 (American Vacuum Society NY, NY, 2019), p. AS-TuP3.
- <sup>14</sup>T. Y. Cho *et al.*, *Thin Solid Films* **660**, 101 (2018).
- <sup>15</sup>B. B. Sahu, S. H. Kim, J. S. Lee, and J. G. Han, *Vacuum* **160**, 316 (2019).
- <sup>16</sup>P. Wang *et al.*, *J. Phys. D: Appl. Phys.* **52**, 345102 (2019).
- <sup>17</sup>Y. Y. Kim, *Korean J. Mater. Res.* **29**, 547 (2019).
- <sup>18</sup>K. P. Lim *et al.*, *IEEE Trans. Magn.* **53**(5), 2900307 (2017).
- <sup>19</sup>S. Kuk, H. K. Nam, Z. Wang, and D. J. Hwang, *J. Nanosci. Nanotechnol.* **18**, 7085 (2018).
- <sup>20</sup>T. Goto, S. Kobayashi, Y. Yabuta, and S. Sugawa, *ECS J. Solid State Sci. Technol.* **8**, N113 (2019).
- <sup>21</sup>R. A. Ovanessian *et al.*, *J. Vac. Sci. Technol. A* **37**, 060904 (2019).
- <sup>22</sup>J. Han, Y. J. Yin, D. Han, and L. Dong, *Mater. Res. Express* **4**, 096301 (2017).
- <sup>23</sup>K. Ohdaira, T. T. Cham, and H. Matsumura, *Jpn. J. Appl. Phys.* **56**, 102301 (2017).
- <sup>24</sup>T. S. Stokkan, H. Haug, C. K. Tang, E. S. Marstein, and J. Gran, *J. Appl. Phys.* **124**, 214502 (2018).
- <sup>25</sup>B. Arkles, Y. Pan, and F. Jove, EP 3274354 B1 (July 3, 2019).
- <sup>26</sup>B. Arkles, *J. Electrochem. Soc.* **133**(1), 233 (1986).
- <sup>27</sup>B. Arkles, C. Brick, J. Goff, and A. E. Kaloyeros, *Thin Solid Films* **711**, 138299 (2020).
- <sup>28</sup>J. Goff, C. Brick, B. Arkles, and A. E. Kaloyeros, *ECS Trans.* **98**, 121 (2020).
- <sup>29</sup>H.-Y. Shih, M.-C. Lin, L.-Y. Chen, and M.-J. Chen, *Nanotechnology* **26**, 014002 (2015).
- <sup>30</sup>P. Motamedi and K. Cadien, *J. Cryst. Growth* **421**, 45 (2015).
- <sup>31</sup>J. M. Park, S. J. Jang, S. I. Lee, and W. J. Lee, *ACS Appl. Mater. Interfaces* **10**, 9155 (2018).